

# Self-Adapting Hydrogel to Improve the Therapeutic Effect in Wound-Healing

Yongsan Li,<sup>†,‡</sup> Xing Wang,<sup>\*,†,‡</sup> Ya-nan Fu,<sup>†</sup> Yen Wei,<sup>‡</sup> Lingyun Zhao,<sup>\*,§</sup> and Lei Tao<sup>\*,†,‡</sup>

<sup>†</sup>Beijing Laboratory of Biomedical Materials, Beijing University of Chemical Technology, Beijing 100029, P. R. China

<sup>‡</sup>Key Laboratory of Bioorganic Phosphorus Chemistry and Chemical Biology (Ministry of Education), Department of Chemistry and <sup>§</sup>Key Laboratory of Advanced Materials, Ministry of Education, Institute of Regenerative Medicine and Biomimetic Material Science and Technology, Tsinghua University, Beijing 100084, P. R. China

## Supporting Information

**ABSTRACT:** Smart materials that can respond to multi-stimuli have been broadly studied. However, the smart materials that can spontaneously answer the ever-changing inner environment of living bodies have not been reported. Here, we report a strategy based on the dynamic chemistry to develop possible self-adapting solid materials that can automatically change shape without external stimuli, as organisms do. The self-adapting property of a chitosan-based self-healing hydrogel has been rediscovered since its dynamic Schiff-base network confers the unique mobility to that solid gel. As a result, the hydrogel can move slowly, like an octopus climbing through a narrow channel, only following the natural forces of surface tension and gravity. The fascinating self-adapting feature enables this hydrogel as an excellent drug carrier for the in vivo wound treatment. In a healing process of the rat-liver laceration, this self-adapting hydrogel demonstrated remarkable superiority over traditional drug delivery methods, suggesting the great potential of this self-adapting hydrogel as a promising new material for biomedical applications. We believe the current research revealed a possible strategy to achieve self-adapting materials and may pave the way toward the further development, study, and application of new-generation smart materials.

**KEYWORDS:** self-adapting materials, hydrogel, drug delivery, wound-healing, dynamic linkage, Schiff base



## INTRODUCTION

Smart materials can respond to multiple external stimuli; thus, the property/function of the smart materials can be tuned according to different needs, leading to improved application effects and broader application areas compared to those of traditional materials.<sup>1–9</sup> With the development of material science, more and more smart materials have been used in biomedical areas for drug delivery,<sup>10–13</sup> three-dimensional (3D) cell culture,<sup>14–16</sup> tissue engineering,<sup>17–20</sup> and biosensing,<sup>21,22</sup> demonstrating the great vitality of smart materials in interdisciplinary fields. On the other hand, the sophisticated in vivo environment also puts forward new requirements to the smart materials. For example, to treat in vivo wounds, a complete fit between the wound and dressing materials is desired for the contact and release of contained medicines. However, the ever-varying inner tissues make it difficult for the dressing materials to keep complete contact with the wound, leading to the unsatisfied therapy effect. Additionally, given the difficulty to introduce external stimuli to the in vivo environment, the development of a biocompatible self-adapting material which can automatically adapt to the changing environment is of significance for wound-healing

and will be a new challenge in both fundamental research and practical applications (Scheme 1A).

The behavior of liquids to fill almost any container under natural conditions due to their movable molecules reveals a possible strategy to design a self-adapting solid. By replacing traditional fixed networks of solid materials with movable linkages, self-adapting materials that have a solid appearance but can move like a liquid under natural conditions might be thereof created.

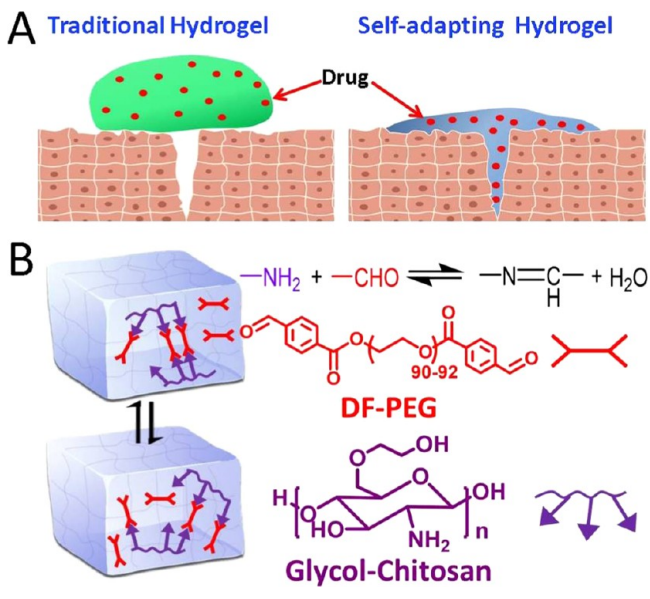
As a concrete example, a biocompatible self-healing hydrogel based on chitosan (CP) and telechelic difunctional poly(ethylene glycol) (DF-PEG)<sup>23,24</sup> that was developed by our group has been tested. The network of this chitosan–PEG hydrogel is constructed through the Schiff base (imine), a well-known dynamic linkage which keeps breakage and regeneration in the aqueous environment of the hydrogel network, resulting in a self-healable hydrogel.<sup>25,26</sup> By deeper study of the construction mechanism of that CP hydrogel, we realized that hydrogel can be considered to be a quasisolid because its

Received: May 29, 2018

Accepted: July 16, 2018

Published: July 16, 2018

Scheme 1. (A) Illustration of the Enhanced Wound-Healing by a Self-Adapting Hydrogel. (B) Schematic Illustration of the Fluid Property of the Solid Hydrogel



dynamic network might allow the hydrogel to move like a very viscous fluid. Thus, it is possible for the hydrogel to move slowly (by changing shape) in the direction of an applied force and rebuild its cross-linked network through the continuous cycle of cleavage and regeneration of the Schiff-base linkages (Scheme 1B), leading to the coveted self-adapting solid material that can change shape under natural forces (the ubiquitous gravity and surface tension). Here, we report the extension upon our previous work to discover several new properties and functions of the CP hydrogel and point toward its potential new applications as a self-adapting material.

## RESULTS AND DISCUSSION

**Escaping Experiment to Verify the Fluidity of the Hydrogel.** To investigate its fluidlike properties, a CP hydrogel containing 0.25% DF-PEG was prepared as per the literature<sup>24</sup> and termed as CP-0.25 hydrogel. The dynamic Schiff-base linkage was verified through a model experiment (Figure S1 and Table S1). The CP-0.25 hydrogel was placed in a glass cuvette (30 mm × 25 mm × 14 mm); then, a curved capillary tube (diameter: 1 mm; length: 24 mm) was inserted (Figure 1). Just under natural condition without any external assistance, the hydrogel was found to spontaneously enter the hollow capillary (Figure 1A1) and gradually move along the tube (Figure 1A2,A3) until finally emerging from the other side of the tube (~46 min, Figure 1A4).

This autonomic movement of the hydrogel is similar to the voluntary behavior of an octopus escaping from a bottle. The hydrogel remained as an integrated solid throughout the process, and the escaped hydrogel (Figure 1A4, inset) exhibited a shear storage modulus ( $G' \sim 550$  Pa) similar to that of the original hydrogel ( $G' \sim 560$  Pa) (Figure 1B), demonstrating the interesting “self-motivation” of an artificial solid hydrogel-like organism.

**Gravity and Capillary Experiments.** The CP-0.25 hydrogel moved only along the natural forces of gravity and surface tension; therefore, the influence of both forces on the hydrogel movement was studied respectively. The effect of

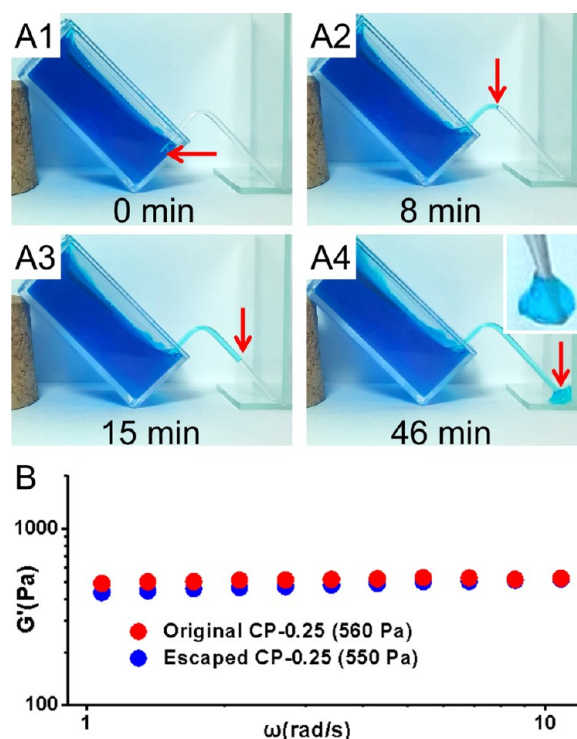


**Figure 1.** (A1–A4) Photographs of the CP-0.25 hydrogel escaping from a cuvette at various time points. (B) Shear storage moduli of the escaped hydrogel (blue) and the original hydrogel (red) (0.1% strain and 6.3 rad/s).

gravity on the movement of the CP-0.25 hydrogel is shown in Figure 2. The hydrogel (1 mL, blue) was placed on the top of a layer of yellow beads (diameter: 6 mm). As a control, a reduced CP-0.25 hydrogel (Re-CP-0.25, green) was prepared by reducing the Schiff-base linkages with  $\text{NaCNBH}_3$  to convert the dynamic network of hydrogel to a fixed skeleton. The CP-0.25 hydrogel (left bottle in Figure 2A1) slowly moved down (under gravity) and engulfed the yellow beads (Figure 2A2) to finally completely fill the narrow space surrounding the beads (Figure 2A3,A3'), demonstrating its automatic mobility. In contrast, the control Re-CP-0.25 hydrogel (right bottle in Figure 2A2) remained on top of the beads even though it is softer ( $G' \sim 320$  Pa, Figure 2B) than the CP-0.25 hydrogel ( $G' \sim 560$  Pa, Figure 2B), suggesting that the dynamic network, rather than the softness, contributes to the mobility of the CP hydrogel.

A capillary experiment was also performed because capillarity is normally observed with liquids under natural conditions (Figure S2). The CP-0.25 hydrogel clearly exhibited capillary (Figure S2B blue) despite its solid appearance (Figure S2A blue), and the Re-CP-0.25 hydrogel (Figure S2B green) barely entered the capillary tube due to the lack of mobility after the reduction of the imine linkages to N–C bonds, confirming that the inner dynamic network offers the liquid feature of the CP hydrogel.

**Evaluation of Different CP Hydrogels as Drug Carriers.** Because of the unique mobility, the self-adapting hydrogel can change shape to much better match the shape of containers or irregular surfaces than traditional hydrogel. Thus, when employed as a drug-carrier, a self-adapting hydrogel can change its shape according to the constantly changing environment of living tissues, to seamlessly adhere to irregular

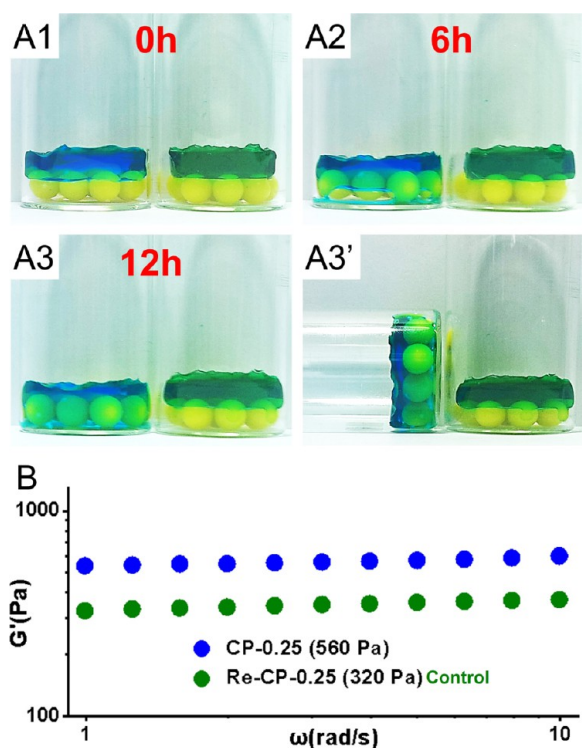


**Figure 2.** (A1–A3') Gravity driving the movement of the CP-0.25 hydrogel (left, blue) and Re-CP-0.25 hydrogel (right, green) with a fixed network as the control. (B) Shear storage moduli of the CP-0.25 hydrogel (blue) and the Re-CP-0.25 hydrogel (green) (0.1% strain and 6.3 rad/s).

tissue surfaces, potentially leading to much better drug delivery and therapeutic outcomes than traditional treatments<sup>10–12,17</sup> (Scheme 1A). Therefore, we prepared three CP hydrogels with different moduli by using different ratios of DF-PEG (0.63,

1.25, 2.50%). These hydrogels were termed as CP-0.63, CP-1.25, and CP-2.50, respectively; their properties were evaluated according to different criteria of drug carriers.

**Self-Adaptability.** To test whether the strengthened hydrogels still possess self-adaptability, the shear-thinning property of these three hydrogels was studied via a step-changing strain experiment (Figure 3A). Hydrogels were tested under alternatively changed shearing strains, as described in previous papers.<sup>23,24</sup> The  $G''$  overpassed the  $G'$  with a high strain value (200%), indicating the breakage of the inner structure of the hydrogels. With a low strain value (1%), the  $G'$  and  $G''$  restored to original values, demonstrating the recovery of the inner structure. Different hydrogels had a similar shear-thinning feature but different shear storage modulus (1.2–4.0 kPa), suggesting the modulus of this self-adapting hydrogel can be simply adjusted according to different application requirements. Three CP hydrogels were put into syringes and injected out, respectively; the broken hydrogel pieces reunited as whole gels after  $\sim 2$  h. The reunited hydrogel followed the containers' shape, suggesting their self-adaptability in spite of higher moduli (Figure 3B). This demonstrated the self-adaptability of CP hydrogels due to the dynamic Schiff-base linkages.

**Biocompatibility Tests.** As a drug carrier, hydrogel should be biocompatible for biomedical usage. Thus, 3D cell culture experiments were carried out to evaluate the bio-safety of CP hydrogels (CP-2.50, CP-1.25, and CP-0.63). L929 (fibroblast) and Hela cells ( $1.5 \times 10^6$  cells/mL) were encapsulated in different CP hydrogels and cultured for 24 h, respectively. Cells were dyed with fluorescein diacetate (FDA) and propidium iodide (PI) before confocal imaging. All cells retained high viability (green dots) after a 24 h culture; only a few dead cells (red dots) were observed in the dyed confocal images (Figure 4A,B). Alamar blue was used to quantitatively evaluate the cytotoxicity of the gels. Both L929 and Hela cells

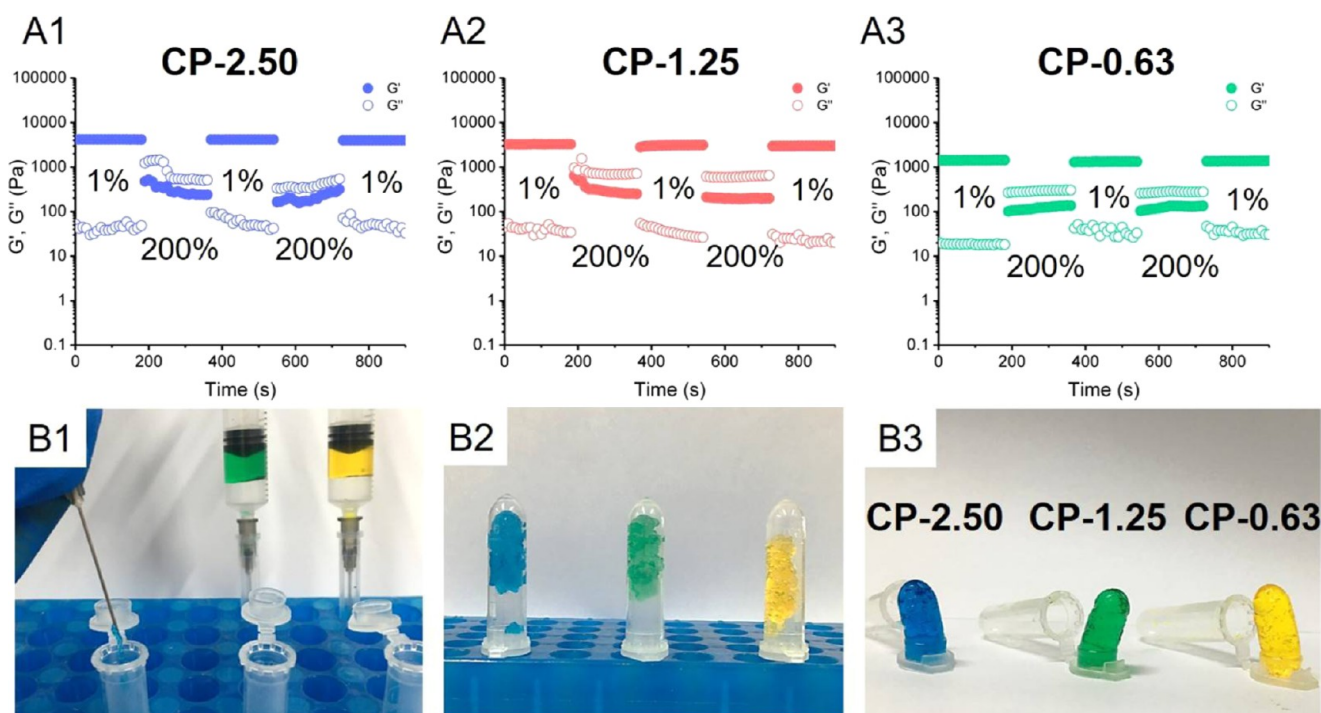


**Figure 3.** (A)  $G'$  and  $G''$  of different CP hydrogels in step-changing strain measurements. (B) Self-adapting experiment of the CP hydrogels.

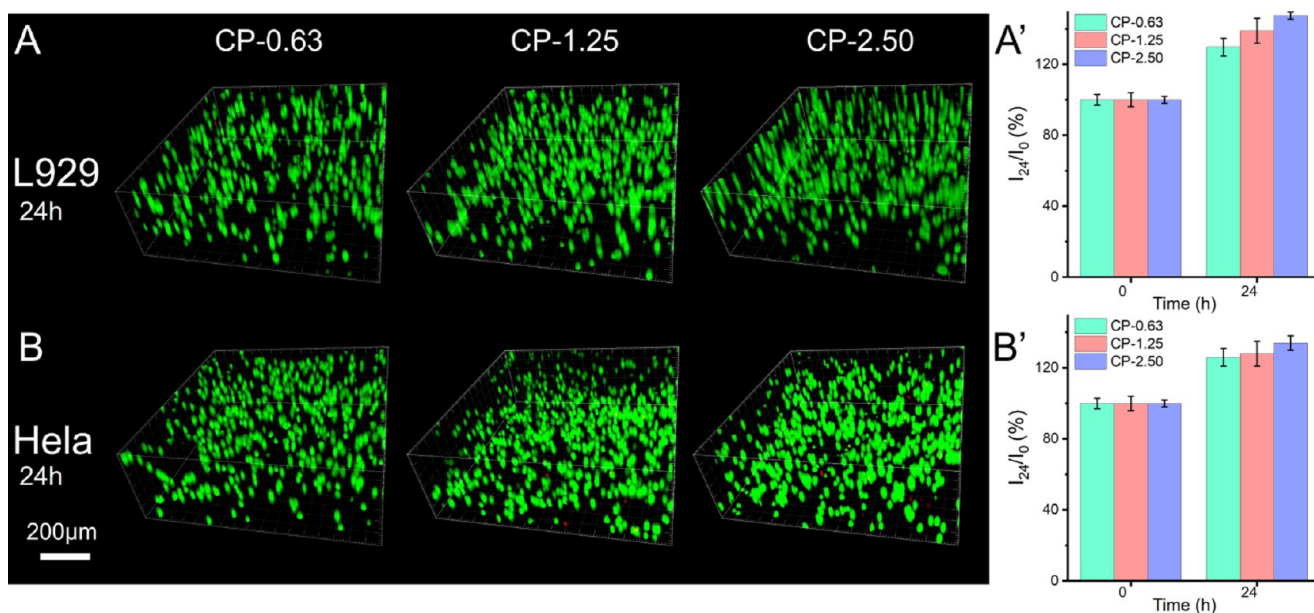


**Figure 4.** Confocal images of (A) L929 cells and (B) HeLa cells (after FDA/PI staining) in hydrogels with different DF-PEG ratios, in a 24 h culture. The viability of (A') L929 cells and (B') HeLa cells in CP hydrogels, alamar blue was used, in a 24 h culture.

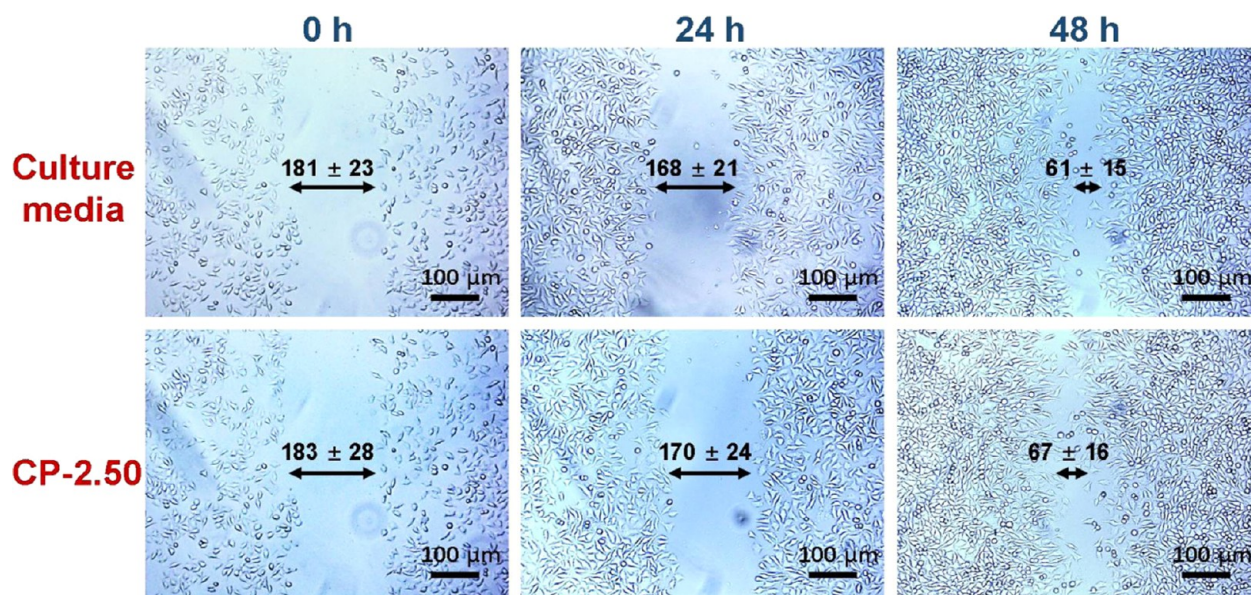


**Figure 5.** Optical images of the in vitro wound-healing experiment (the CP-2.50 hydrogel as an example).

grew well in hydrogels, suggesting the satisfactory biocompatibility of all CP hydrogels (Figure 4A',B').

**In Vitro Wound-Healing Tests.** The CP hydrogel was used as a model of wound-dressing in a preliminary in vitro test. L929 cells were cultured in a Petri dish; then, an artificial wound was created by scratching the dish with a 200 μL pipette tip. The artificial wounds were covered by CP hydrogel (the CP-2.50 hydrogel as an example). Cells in Roswell Park Memorial Institute (RPMI) 1640 culture media served as the control. Both wounds were covered by cells in the following 48 h culture (Figure 5), suggesting the hydrogel as a potential wound-dressing material.

Subsequently, the CP hydrogel was combined with thrombin (a model drug) by simply dissolving thrombin in an aqueous DF-PEG solution and then mixing with glycol chitosan solution. This CP hydrogel/thrombin was defined as

the “CPT hydrogel”. With different DF-PEG ratios, the CPT hydrogels were termed as CPT-0.63, CPT-1.25, and CPT-2.50, respectively. These hydrogels were tested according to the clinical requirements to screen the best candidate for internal injury.

**Tissue Mucoadhesive Ability.** The tissue mucoadhesive ability of the CPT hydrogels was assessed according to the standard protocol (ASTM F2258-05) using a tensiometer (DCAT 21) (Figure 6A, porcine intestine as the mucous tissue). The mass–distance curves were recorded (Figure 6B), and the adhesiveness of all CPT hydrogels on porcine intestine ranged from 0.9 to 1.1 kPa (Figure 6B), satisfying the requirement of adhering to tissues.<sup>27</sup> However, the reduced gels showed lower adhesiveness than that of the original ones (~0.6–0.8 kPa, Figure S4).

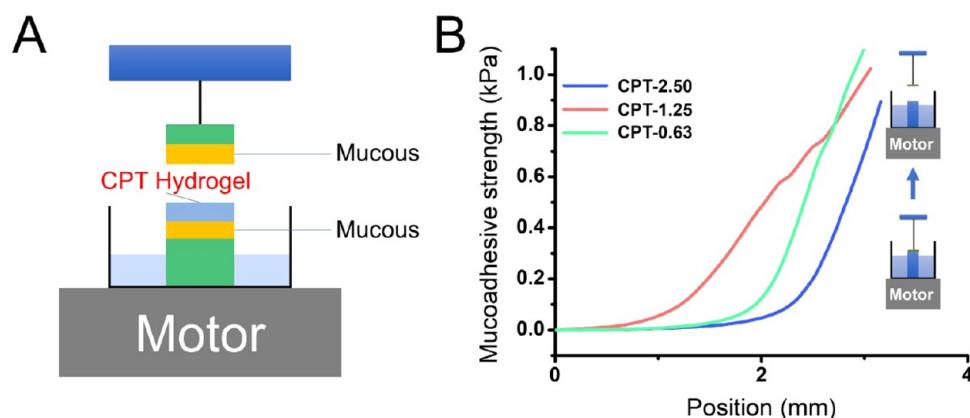


**Figure 6.** (A) Test system for evaluating the tissue adhesive strength of the CPT hydrogels. (B) Mucoadhesive strength of the different CPT hydrogels. Motor speed: 1.0 mm/s.

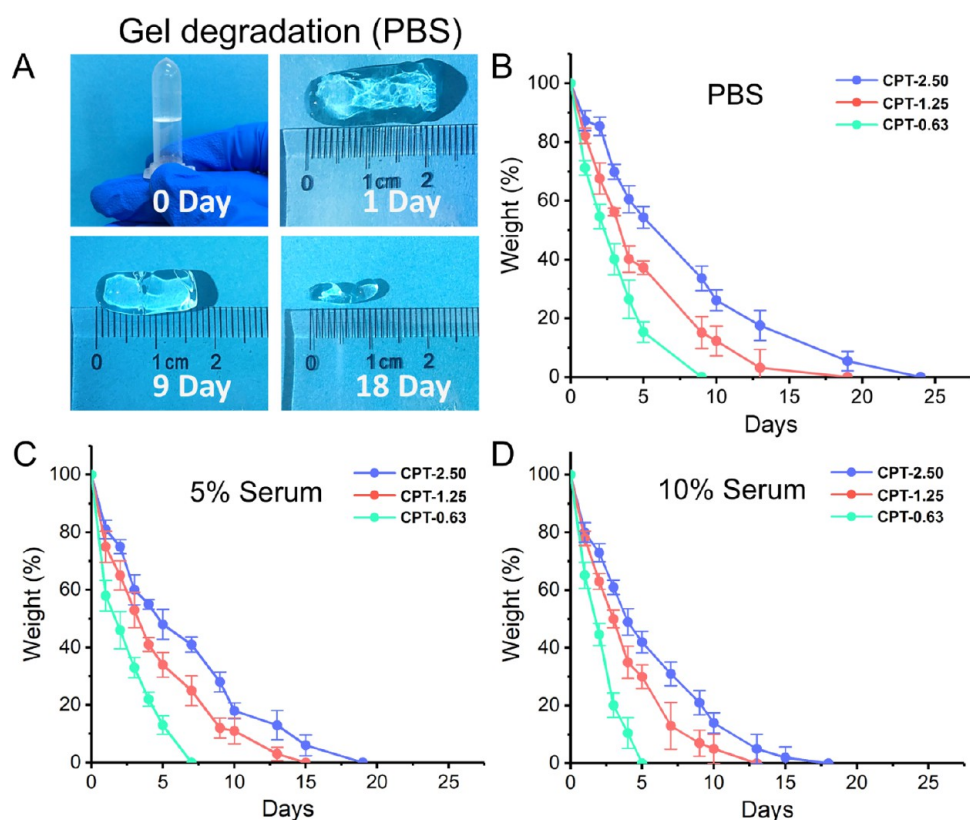


**Figure 7.** (A) Remaining hydrogels at different time points (CPT-2.50 as an example). The weight–time curves of the CPT hydrogels during the degradation experiment in (B) PBS, (C) 5% serum, and (D) 10% serum. Data were presented as means  $\pm$  standard deviation ( $n = 6$ ).

**In Vitro Degradation.** Wound-dressing should be biodegradable to treat internal injury; thus, the CPT hydrogels were tested via an in vitro degradation experiment. Three CPT hydrogels were incubated in 10 mL of phosphate-buffered saline (PBS) solution and kept in a shaker (37 °C, 700 rpm), respectively. Hydrogels were taken out at different time points and weighted. The degradation of hydrogel could be directly observed (Figure 7A, the CPT-2.50 as an example); the CPT-2.50 hydrogel degraded much slower ( $\sim 24$  days) than the counterparts (CPT-0.63, CPT-1.25) ( $\sim 9$ , 19 days) (Figure 7B). This suggests the CPT-2.50 hydrogel is the best for long-term treatment. Meanwhile, the degradation behaviors of gels in serum solutions (5, 10% in PBS) were also studied, respectively. The gels in serum solutions degraded faster than

those in pure PBS, whereas no obvious difference was noticed in 5 and 10% serum solutions (Figure 7C,D). Furthermore, cytotoxicity of the degradation products (glycol chitosan and DF-PEG) was studied. Cells survived well ( $\sim 80\%$ ) after 24 h culture with 16 mg/mL glycol chitosan or DF-PEG (Figure S5), confirming the biocompatibility of the CP hydrogels.

**Cumulative Release of the Thrombin.** All CPT hydrogels were immersed in PBS solutions for communitive release study, respectively (Figure 8). The encapsulated thrombin gradually released until the complete degradation of the hydrogel. For CPT-0.63 hydrogel, the drug rapidly released ( $\sim 98\%$ ) in 9 days. On the other hand, CPT-2.50 hydrogel held the longest release time ( $\sim 24$  days).

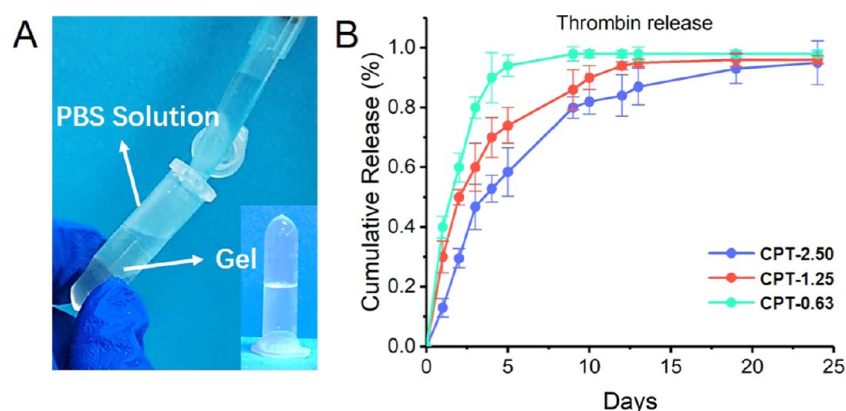
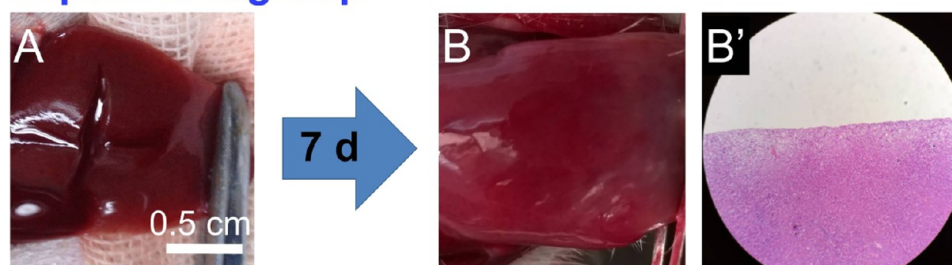


**Figure 8.** (A) Experimental setup of the cumulative release of thrombin from the CPT hydrogel. (B) The cumulative released thrombin vs time; data were presented as means  $\pm$  standard deviation ( $n = 6$ ).

### Experiment group



**CPT-2.50**

### Control groups

No treatment    Thr-H<sub>2</sub>O    FT hydrogel    CP-2.50

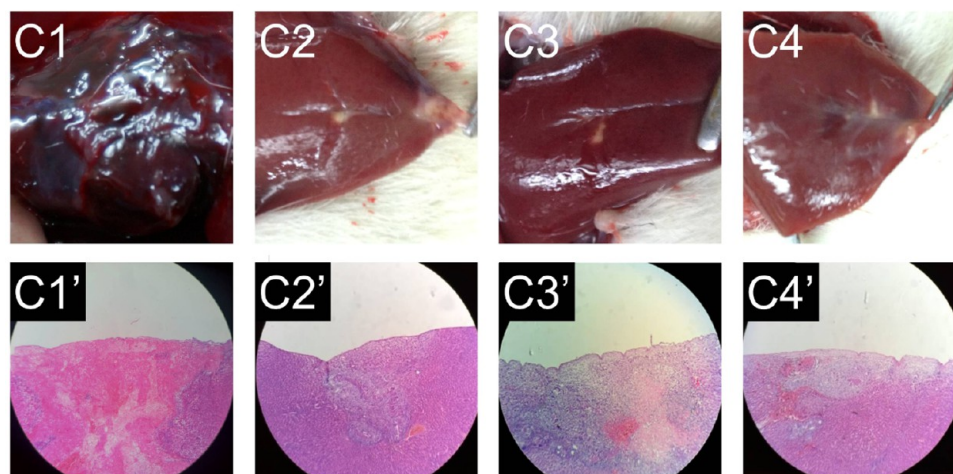


**Figure 9.** Photographs and microscopic evaluation of rat liver laceration with different treatments. (A) The cross-shaped incision wound. (B, B') Wound-healing after 7 days by the treatment of CPT hydrogel. (C) Wound progression after 7 days in control rats: (C1, C1') no treatment; (C2, C2'): treatment with an aqueous solution of thrombin; (C3, C3'): treatment with F127 hydrogel containing thrombin; (C4, C4'): treatment with CP-2.50 ( $n = 6$ ).

As a result, the CPT-2.50 hydrogel was chosen for the next study because of its excellent performance in adhesion, degradation, drug release, and biocompatibility. Meanwhile, the gelation time of the CPT-2.50 hydrogel is within 2 min (Figure S3A), matching the time scales of hemostasis and related clinical applications.<sup>28,29</sup> Moreover, the shear storage modulus of the selected CPT-2.50 was approximately 4.0 kPa

(Figure S3B), similar to the mechanical strength of liver tissue.<sup>18,30</sup>

**In Vivo Wound-Healing Tests.** The optimized CPT hydrogel (CPT-2.50) has been used to treat hemorrhaging livers in rats following the reported protocol.<sup>19,20</sup> Briefly, a cruciate incision (length: 1.0 cm, depth: 0.3 cm) was made by a surgical scalpel on the right lobe of a rat liver (Figure 9A) to yield a liver laceration of grade VI.<sup>31</sup> After directly spreading

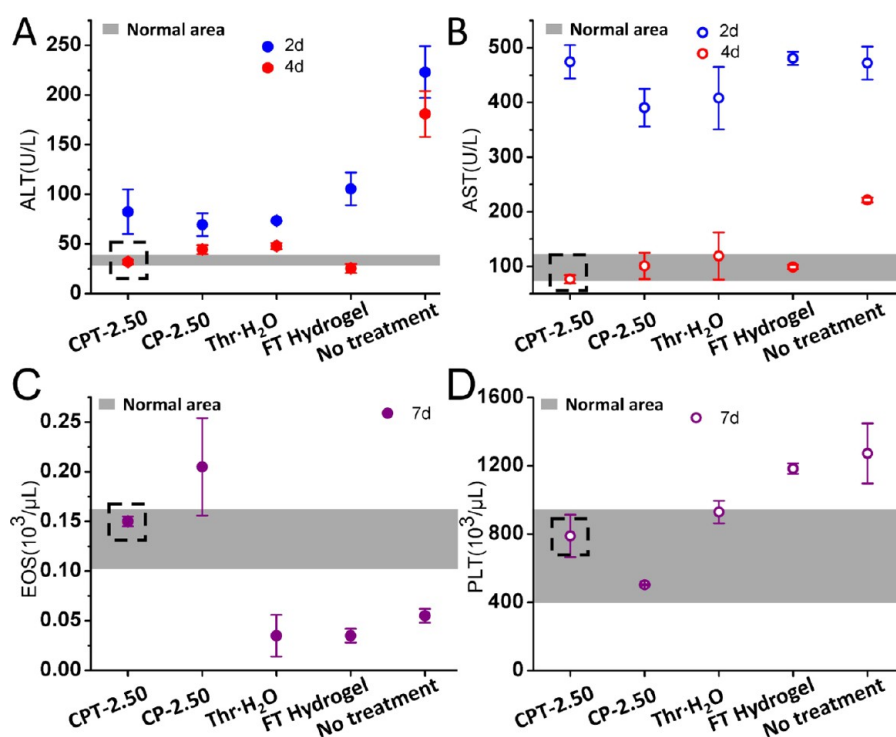


**Figure 10.** Clinical chemistry and hematological analyses indices of rats, on the 2nd and 4th day after surgery: (A) alanine aminotransferase (ALT) and (B) aspartate aminotransferase (AST) and (C) eosinophils (EOS) and (D) platelet (PLT). Gray areas represent the control data obtained from the Charles River. Data were presented as means  $\pm$  standard deviation ( $n = 6$ ).

the CPT-2.50 hydrogel onto the wound, the bleeding ceased within 2 min, demonstrating the excellent hemostatic effect of the CPT hydrogel during surgery. Afterward, the opened abdomen was stitched and all treated rats were freed as the standard process. During the observation period (7 days), the rats survived well with decreased and then increased weights (Figure S7), indicating the rats gradually recovered after operation. Then, the rats were sacrificed to evaluate the effect of wound-healing. Upon visual inspection, the post-treatment liver capsule appeared with a smooth surface and healthy color (Figure 9B), preliminarily indicating complete healing of the liver incisions and excellent tissue regeneration. Detailed evaluations were further obtained by the histology analysis. After staining with haematoxylin and eosin (H&E), it is clear that the regenerated hepatocytes possessed the same level of organization as normal tissue (Figure 9B') and no obvious inflammatory cell infiltration or necrosis occurred in the regenerated tissue (Figure S8A), confirming the excellent therapy effect of wound-healing using the CPT hydrogel as the drug carrier.

Rats with the same surgery but several other treatments were employed as positive controls. The treatments were thrombin aqueous solution (Thr·H<sub>2</sub>O), Plurionic (F127) hydrogel containing thrombin (F127-thrombin (FT) hydrogel), and CP-2.50 without thrombin. Liver-lacerated rats that received no treatment were used as negative controls (Figure 9C). Although all positive control groups showed much shorter bleeding times (3–5 min) than those of the negative group (>10 min), none of them was as fast as the CPT hydrogel.

After 7 days, blood clots and mangled wounds could be clearly observed (Figure 9C1) in the negative control group (without treatment) and large areas of hepatocellular necrosis could be found in the microscopic histology analyses (Figure 9C1').

In all positive control groups (Figure 9C2–C4), scars remained distinctly visible although they healed much better than those in the negative group. Specifically, comparisons of the histology results (Figures 9B',C' and S8) between the positive controls and treated rats using CPT hydrogel revealed that the thrombin-solution treatment partially healed the wound (Figure 9C2) but some areas of eosinophilic cytoplasm and dense inflammatory cells were still visible (Figure 9C2'), suggesting the unsatisfactory effect by the traditional treatment. It is noticeable the FT hydrogel (Figure 9C3') exhibited even worse effects than with the thrombin solution (Figure 9C2'), which might be caused by the poor fluidity of the non-self-adapting F127 hydrogel, leading to nonideal contact between the drug and the wound surface and weakened therapeutic effect of the infused drug (Scheme 1B). Meanwhile, the CP hydrogel also displayed a remedial effect as a hemostat (Figure 9C4'), verifying that the CP hydrogel is a suitable basic material for wound-healing because of its physical adhesion to the wound and using the natural anti-inflammatory chitosan as a gelator.<sup>32,33</sup>

Further assays, including the biochemical indices of blood and hematological analyses indices (Figure 10) were also carried out. Figure 10A,B demonstrated the biochemical indices of blood samples collected on the 2nd and 4th day after the treatments. On the 2nd day, alanine aminotransferase (ALT) and aspartate aminotransferase (AST) levels increased to quite high levels, but on the 4th day, all indices fell to normal or near-normal levels (the gray areas, on the basis of data from healthy rats), suggesting that all treatments were safe for the animals. It is noticeable that in the untreated group, the indices remained elevated, indicating an abnormal condition of the rats.

Hematological analysis of rats was carried out on the 7th day after treatment, and two key parameters (eosinophils (EOS)

and platelet (PLT) count) were recorded to evaluate the significant differences of different treatments (Figure 10C,D). Figure 10C indicated that the EOS index matched the healthy range (by the Charles River) only in the CPT hydrogel group. The rats treated with CP hydrogel group exhibited slightly higher values, and other groups exhibited far lower indices. PLT indices of the rats treated by the CPT hydrogel, the CP hydrogel, and the thrombin solution were in good condition (Figure 10D). Higher levels of the PLT indices were observed in the untreated rats and FT hydrogel-treated rats. All of these data suggested that the hematological healing effect after the treatment with the CPT hydrogel was superior to all other methods, confirming that a suitable drug carrier is extremely important for realizing the function of pharmacological drug and the best therapeutic effect.<sup>34,35</sup>

## CONCLUSIONS

In summary, we present a new aspect, self-adaptability, of an established hydrogel by deeply understanding the inner mechanism of the material. As a result, a self-healing hydrogel constructed through the dynamic Schiff-base linkages has been upgraded as a self-adapting hydrogel that can change shape and move autonomously under natural conditions like organisms do. The dynamic linkages confer the solid hydrogel a fluidlike mobility that has a unique advantage as a drug carrier to locate drugs to wound sites. In the *in vivo* wound-healing experiment, the hydrogel exhibited unequalled therapeutic effect than that of other control treatments, directly demonstrating the advantage of self-adapting material for drug delivery. Given most living tissues exist in the constantly changing *in vivo* environment where it is difficult to introduce external stimuli, it is almost impossible for traditional smart biomaterials to change their shapes and positions to adapt the internal tissue environment. Self-adapting hydrogels may offer a promising alternative to deliver drugs to internal environment and open up several new applications in embolotherapy, joint lubrication, cartilage therapy etc.

Besides imine, several other dynamic chemical linkages (disulfide, acetal, hydrazine, ester, etc.) and physical interactions (charge, hydrogen bond, and supramolecular recognition) have been broadly studied to construct diverse self-healing materials.<sup>36–40</sup> Such materials may also be able to be further upgraded to self-adapting materials according to the perspectives presented in the current research. For example, the self-healing materials with metal–ligand coordination as inner dynamic linkages<sup>2,3</sup> might also be upgraded as self-adapting materials to mimic muscle behaviors. We believe the deeper understanding of the internal construction mechanism of existing materials should be an efficient approach to exploit new materials, which might lead to the rediscovery of a new property/function of known materials for applications in new areas.

## MATERIALS AND METHODS

**Reagents and Chemicals.** DF-PEG ( $M_n \sim 4000$  g/mol) was synthesized following a procedure mentioned in our previous study.<sup>23</sup> Glycol chitosan (Wako Pure Chemical Industries, 90% degree of deacetylation), Pluronic F127 (Sinopharm Chemical Reagent), 4-carboxybenzaldehyde (Aladdin, 99%), *N,N'*-dicyclohexylcarbodiimide (Aladdin, 99%), 4-dimethylamopyridine (Aladdin, 99%), and PEG (Sinopharm Chemical Reagent,  $M_n \sim 4000$ ) were used as purchased. Thrombin was ordered from Changchun Yuandaguao Pharm. All solvents were purchased from Sinopharm Chemical Reagent and used

directly without further purification. Rats (SD) were purchased from the Charles River. Other agents were purchased from Sinopharm and used without further purification.

**Characterizations.** <sup>1</sup>H NMR spectra were obtained using a JEOL JNM-ECA400 (400 MHz) spectrometer for all samples. The rheology analysis was carried out using an AR-2 rheometer with parallel plate geometry (20 mm in diameter). The mucoadhesive test was carried out using a DCAT 21 tensiometer, followed by a modified standard test method for strength properties of tissue adhesives in tension (ASTM F2258-05) method. The H&E histological pictures were captured by a Leica DM3000 B microscope. All *in vivo* tests were performed under the technical guidelines for nonclinical study issued by China Food and Drug Administration and authorized by the ethics committee of Cancer Hospital, Chinese Academy of Medical Science.

**Methods. Preparation of the CP-0.25 and the Re-CP-0.25.** DF-PEG (0.01 g) was dissolved in deionized water (0.99 g), and glycol chitosan (0.09 g) was dissolved in deionized water (2.91 g). The CP hydrogel was then prepared by mixing the two solutions at 25 °C to yield a CP hydrogel containing 2.25% (w/w) glycol chitosan and 0.25% (w/w) DF-PEG.

The Re-CP-0.25 was prepared by reducing the CP-0.25 hydrogel with NaBH<sub>3</sub>CN aqueous solution (0.20 mL, 0.4%).

**Step-Changing Rheology Tests.** CP hydrogels (400 μL) with different concentrations of DF-PEG were prepared and placed on the parallel plate of the rheometer, respectively. Low strain (1%, 3 min) and high strain (200%, 3 min) were performed alternately to observe the hydrogels.

**Biocompatibility of the Hydrogels (Qualitative).** L929 cells were resuspended in a glycol chitosan solution (0.0225 g of GCS in 0.8 mL of RPMI 1640 culture media), then mixed with a DF-PEG solution (0.0250 g of DF-PEG in 0.2 mL of RPMI 1640 culture media) in a confocal dish and covered with 1.0 mL of RPMI 1640 culture media. After 24 h, the cells were stained with fluorescein diacetate (FDA) and propidium iodide (PI) for 10 min prior to observation. Other CP hydrogels were similarly tested.

**Biocompatibility of the Hydrogels (Quantitative).** Cell-loading gels were incubated with alamar blue (5% in RPMI 1640 medium) for 6 h, then the fluorescence of the supernatant was tested ( $E_e$ : 575 nm;  $E_m$ : 605 nm). Cell-loading gels were tested at 0 and 24 h, respectively; the fluorescent emission ratio ( $I_{24}/I_0$ ) was recorded to assess the biocompatibility of the hydrogel.

**In Vitro Wound-Healing Tests.** To evaluate the wound-healing ability of the CP-2.50 hydrogel, an *in vitro* test was carried out. L929 cells (a fibroblast cell line) were cultured in a Petri dish (diameter 3.5 mm); then, an artificial wound was created by scratching the bottom of the dish with a 200 μL pipette tip. The cells were washed with PBS. The artificial wound was covered by 1 mL of CP-2.50 hydrogel and 1 mL of RPMI 1640 culture media, respectively, followed by a 48 h observation. Optical images were taken at different time points to observe the healing process.

**Preparation of the CPT-2.50.** DF-PEG/thrombin solutions were first obtained by dissolving DF-PEG (0.10 g) and thrombin (0.05 g) in 0.85 g of deionized water. CPT-2.50 hydrogels were then prepared through simply mixing the above-mentioned solutions with glycol chitosan solution, which finally contained 2.25% (w/w) glycol chitosan, 1.25% (w/w) thrombin, and 2.50% (w/w) DF-PEG.

**Mucoadhesive Tests.** The tissue mucoadhesive strength of the CPT hydrogel was assessed according to the standard test method for strength properties of tissue adhesives in tension (ASTM F2258-05) using a tensiometer (DCAT 21) to record mass–distance curves and porcine intestine as the mucous tissue (Figure 6A). The intestine was cleaned and cut to a suitable size and shape, then fixed to substrates and maintained at 37 °C in a humid environment. The solution was applied to the prepared intestinal tissue surface (bonding area: 314 mm<sup>2</sup>); then, the motor was driven upward (position 3–0 mm) to touch the upper mucous membrane. When the difference in the detected mass exceeded 100 mg, the motor was further driven upward by a distance of 3.5 mm (position 0 to –3.5 mm) to ensure sufficient contact between both pieces of intestine and the solution. After 5 min, the CPT hydrogel was fully converted to hydrogel; the motor was

driven downward to carry out the detaching step. The bonded mucous tissues were loaded until complete separation (motor speed  $\sim 1.0$  mm/s). The attaching/detaching cycles were recorded, and the maximum mass in the mass–distance curve presented the dissociation force of the mucoadhesive strength (Figure 4B). The mucoadhesiveness of the CPT hydrogel used in the animal tests was calculated to be approximately 0.9 kPa.

**In Vitro Degradation Tests.** The CPT-2.50 hydrogel (1 mL) was submerged in 10 mL of PBS solution (0.01%) and kept in a shaker (37 °C, 700 rpm). The weight of the remaining hydrogel was weighed everyday ( $n = 6$ ). Other CPT hydrogels were similarly tested.

**Cumulative Release Test.** The CPT-2.50 hydrogel (1 mL) was submerged in 10 mL of PBS solution (0.01%) and kept in a shaker (37 °C, 700 rpm). The released thrombin was detected using a UV–vis meter (280 nm) every other day. Other CPT hydrogels were similarly tested.

**Hematological Tests.** The aspartate transaminase (AST) and alanine transaminase (ALT) activities were measured in each mouse blood sample with the AST/ALT kit from Biosino Bio-Technology and Science Incorporation.

**Statistical Analyses.** All data were shown with mean  $\pm$  standard deviation. Six parallel tests were carried out in each experiment.

## ■ ASSOCIATED CONTENT

### Supporting Information

The Supporting Information is available free of charge on the ACS Publications website at DOI: 10.1021/acsami.8b08874.

<sup>1</sup>H NMR spectrum of Schiff base, capillarity experiments, rheology analyses, mucoadhesiveness test, cytotoxicity test, swelling ratio of the hydrogels, rat weight changes, H&E histological examination (PDF)

## ■ AUTHOR INFORMATION

### Corresponding Authors

\*E-mail: wangxing@mail.buct.edu.cn (X.W.).

\*E-mail: lyzhao@mail.tsinghua.edu.cn (L.Z.).

\*E-mail: leitao@mail.tsinghua.edu.cn (L.T.).

### ORCID

Xing Wang: 0000-0002-9990-1479

Lei Tao: 0000-0002-1735-6586

### Notes

The authors declare no competing financial interest.

## ■ ACKNOWLEDGMENTS

The authors acknowledge the National Natural Science Foundation of China (21574008, 21474057, and 21574073) for their funding support. Valuable discussions with Prof. T. D. Zhao (PhD, M.D.) at the China–Japan Friendship Hospital are appreciated.

## ■ REFERENCES

- (1) Lai, J.-C.; Mei, J.; Jia, X.; Li, C.; You, X.; Bao, Z. A Stiff and Healable Polymer Based on Dynamic - Covalent Boroxine Bonds. *Adv. Mater.* **2016**, *28*, 8277–8282.
- (2) Li, C.-H.; Wang, C.; Keplinger, C.; Zuo, J.; Jin, L.; Sun, Y.; Zheng, P.; Cao, Y.; Lissel, F.; Linder, C.; You, X.; Bao, Z. A Highly Stretchable Autonomous Self-Healing Elastomer. *Nat. Chem.* **2016**, *8*, 618–624.
- (3) Rao, Y.-L.; Chortos, A.; Pfattner, R.; Lissel, F.; Chiu, Y.-C.; Feig, V.; Xu, J.; Kurosawa, T.; Gu, X.; Wang, C.; He, M.; Chung, J.-W.; Bao, Z. Stretchable Self-Healing Polymeric Dielectrics Cross-Linked through Metal–Ligand Coordination. *J. Am. Chem. Soc.* **2016**, *138*, 6020–6027.
- (4) Sun, Y.; Lopez, J.; Lee, H. W.; Liu, N.; Zheng, G.; Wu, C. L.; Sun, J.; Liu, W.; Chung, J. W.; Bao, Z.; Cui, Y. A Stretchable Graphitic

Carbon/Si Anode Enabled by Conformal Coating of a Self - Healing Elastic Polymer. *Adv. Mater.* **2016**, *28*, 2455–2461.

(5) Sun, T. L.; Kurokawa, T.; Kuroda, S.; Ihsan, A. B.; Akasaki, T.; Sato, K.; Haque, M. A.; Nakajima, T.; Gong, J. P. Physical Hydrogels Composed of Polyampholytes Demonstrate High Toughness and Viscoelasticity. *Nat. Mater.* **2013**, *12*, 932–937.

(6) Luo, F.; Sun, T. L.; Nakajima, T.; Kurokawa, T.; Zhao, Y.; Sato, K.; Ihsan, A. B.; Li, X.; Guo, H.; Gong, J. P. Oppositely Charged Polyelectrolytes Form Tough, Self - Healing, and Rebuildable Hydrogels. *Adv. Mater.* **2015**, *27*, 2722–2727.

(7) Ihsan, A. B.; Sun, T. L.; Kurokawa, T.; Karobi, S. N.; Nakajima, T.; Nonoyama, T.; Roy, C. K.; Luo, F.; Gong, J. P. Self-Healing Behaviors of Tough Polyampholyte Hydrogels. *Macromolecules* **2016**, *49*, 4245–4252.

(8) Grinthal, A.; Aizenberg, J. Adaptive All the Way Down: Building Responsive Materials from Hierarchies of Chemomechanical Feedback. *Chem. Soc. Rev.* **2013**, *42*, 7072–7085.

(9) Yao, X.; Hu, Y.; Grinthal, A.; Wong, T.-S.; Mahadevan, L.; Aizenberg, J. Adaptive Fluid-Infused Porous Films with Tunable Transparency and Wettability. *Nat. Mater.* **2013**, *12*, 529–534.

(10) Peppas, N. A.; Hilt, J. Z.; Khademhosseini, A.; Langer, R. Hydrogels in Biology and Medicine: From Molecular Principles to Bionanotechnology. *Adv. Mater.* **2006**, *18*, 1345–1360.

(11) Langer, R.; Tirrell, D. A. Designing Materials for Biology and Medicine. *Nature* **2004**, *428*, 487–492.

(12) Langer, R. Drug Delivery And Targeting. *Nature* **1998**, *392*, 5–10.

(13) Mura, S.; Nicolas, J.; Couvreur, P. Stimuli-Responsive Nanocarriers for Drug Delivery. *Nat. Mater.* **2013**, *12*, 991–1003.

(14) Boyan, B. D.; Hummert, T. W.; Dean, D. D.; Schwartz, Z. Role of Material Surfaces in Regulating Bone and Cartilage Cell Response. *Biomaterials* **1996**, *17*, 137–146.

(15) Lutolf, M. P.; Gilbert, P. M.; Blau, H. M. Designing Materials to Direct Stem-Cell Fate. *Nature* **2009**, *462*, 433–441.

(16) Cushing, M. C.; Anseth, K. S. Hydrogel Cell Cultures. *Science* **2007**, *316*, 1133–1134.

(17) Decker, C. G.; Wang, Y.; Paluck, S. J.; Shen, L.; Loo, J. A.; Levine, A. J.; Miller, L. S.; Maynard, H. D. Fibroblast Growth Factor 2 Dimer with Superagonist in Vitro Activity Improves Granulation Tissue Formation During Wound Healing. *Biomaterials* **2016**, *81*, 157–168.

(18) Lee, K. Y.; Mooney, D. J. Hydrogels for Tissue Engineering. *Chem. Rev.* **2001**, *101*, 1869–1880.

(19) Ryu, J. H.; Lee, Y.; Kong, W. H.; Kim, T. G.; Park, T. G.; Lee, H. Catechol-Functionalized Chitosan/Pluronic Hydrogels for Tissue Adhesives and Hemostatic Materials. *Biomacromolecules* **2011**, *12*, 2653–2659.

(20) Lih, E.; Lee, J. S.; Park, K. M.; Park, K. D. Rapidly Curable Chitosan–Peg Hydrogels as Tissue Adhesives for Hemostasis and Wound Healing. *Acta Biomater.* **2012**, *8*, 3261–3269.

(21) Anker, J. N.; Hall, W. P.; Lyandres, O.; Shah, N. C.; Zhao, J.; Van Duyne, R. P. Biosensing with Plasmonic Nanosensors. *Nat. Mater.* **2008**, *7*, 442–453.

(22) Daniel, M.-C.; Astruc, D. Gold Nanoparticles: Assembly, Supramolecular Chemistry, Quantum-Size-Related Properties, and Applications toward Biology, Catalysis, and Nanotechnology. *Chem. Rev.* **2004**, *104*, 293–346.

(23) Zhang, Y.; Tao, L.; Li, S.; Wei, Y. Synthesis of Multiresponsive and Dynamic Chitosan-Based Hydrogels for Controlled Release of Bioactive Molecules. *Biomacromolecules* **2011**, *12*, 2894–2901.

(24) Yang, B.; Zhang, Y.; Zhang, X.; Tao, L.; Li, S.; Wei, Y. Facilely Prepared Inexpensive and Biocompatible Self-Healing Hydrogel: A New Injectable Cell Therapy Carrier. *Polym. Chem.* **2012**, *3*, 3235–3238.

(25) Roy, N.; Bruchmann, B.; Lehn, J.-M. Dynamers: Dynamic Polymers as Self-Healing Materials. *Chem. Soc. Rev.* **2015**, *44*, 3786–3807.

(26) Yu, G.; Yan, X.; Han, C.; Huang, F. Characterization of Supramolecular Gels. *Chem. Soc. Rev.* **2013**, *42*, 6697–6722.

- (27) Shelke, N. B.; James, R.; Laurencin, C. T.; Kumbar, S. G. Polysaccharide Biomaterials for Drug Delivery and Regenerative Engineering. *Polym. Adv. Technol.* **2014**, *25*, 448–460.
- (28) Gegel, B.; Burgert, J.; Cooley, B.; MacGregor, J.; Myers, J.; Calder, S.; Luellen, R.; Loughren, M.; Johnson, D. The Effects of Bleedarrest, Celox, and Traumadex on Hemorrhage Control in a Porcine Model. *J. Surg. Res.* **2010**, *164*, e125–e129.
- (29) Pusateri, A. E.; Holcomb, J. B.; Kheirabadi, B. S.; Alam, H. B.; Wade, C. E.; Ryan, K. L. Making Sense of the Preclinical Literature on Advanced Hemostatic Products. *J. Trauma: Inj., Infect., Crit. Care* **2006**, *60*, 674–682.
- (30) Trahey, G.; Dumont, D.; Fahey, B. 4K-1 Volume Visualization and Error Analysis Using 3D ARFI Imaging Data. *IEEE Ultrason. Symp.* **2006**, 1140–1143.
- (31) Hollands, M. J.; Little, J. M. The Role of Hepatic Resection in the Management of Blunt Liver Trauma. *World J. Surg.* **1990**, *14*, 478–482.
- (32) Ngo, D.-H.; Vo, T.-S.; Ngo, D.-N.; Kang, K.-H.; Je, J.-Y.; Pham, H. N.-D.; Byun, H.-G.; Kim, S.-K. Biological Effects of Chitosan and Its Derivatives. *Food Hydrocolloids* **2015**, *51*, 200–216.
- (33) Chung, M. J.; Park, J. K.; Park, Y. I. Anti-Inflammatory Effects of Low-Molecular Weight Chitosan Oligosaccharides in Ige–Antigen Complex-Stimulated Rbl-2h3 Cells and Asthma Model Mice. *Int. Immunopharmacol.* **2012**, *12*, 453–459.
- (34) Allen, T. M.; Cullis, P. R. Drug Delivery Systems: Entering the Mainstream. *Science* **2004**, *303*, 1818–1822.
- (35) Kohane, D. S.; Langer, R. Biocompatibility and Drug Delivery Systems. *Chem. Sci.* **2010**, *1*, 441–446.
- (36) Xia, F.; Jiang, L. Bio - Inspired, Smart, Multiscale Interfacial Materials. *Adv. Mater.* **2008**, *20*, 2842–2858.
- (37) He, X.; Aizenberg, M.; Kuksenok, O.; Zarzar, L. D.; Shastri, A.; Balazs, A. C.; Aizenberg, J. Synthetic Homeostatic Materials with Chemo-Mechano-Chemical Self-Regulation. *Nature* **2012**, *487*, 214–218.
- (38) Lehn, J. M. Perspectives in Chemistry—Aspects of Adaptive Chemistry and Materials. *Angew. Chem., Int. Ed.* **2015**, *54*, 3276–3289.
- (39) Lehn, J. M. From Supramolecular Chemistry Towards Constitutional Dynamic Chemistry and Adaptive Chemistry. *Chem. Soc. Rev.* **2007**, *36*, 151–160.
- (40) Ramström, O.; Lehn, J. M. Drug Discovery by Dynamic Combinatorial Libraries. *Nat. Rev. Drug Discovery* **2002**, *1*, 26–36.